Medicinal Chemistry Research (2020) 29:1590–1599
https://doi.org/10.1007/s00044-020-02585-6

MEDICINAL CHEMISTRY RESEARCH

ORIGINAL RESEARCH

Synthesis, radical scavenging, and antioxidant activity of stilbazolic resveratrol analogs

Alexander V. Semenov[1] · Olga I. Balakireva[1] · Irina V. Tarasova[1] · Elena V. Semenova[2] · Polad K. Zulfugarov[2]

Received: 25 March 2020 / Accepted: 3 June 2020 / Published online: 14 June 2020

Abstract

To continue the research on the preparation of resveratrol structural analogs containing the 3-pyridinol fragment, a series of derivatives with an ethyl radical sterically shielding the hydroxyl group was synthesized. It was shown that the ethyl group introduction has an ambiguous effect on the radical scavenging and antioxidant properties of the stilbazoles studied, which is probably related to the structural features of the resulting radical intermediates. The correlation between the radical scavenging and antioxidant properties of the derivatives studied is established. A number of compounds have been identified that exhibit an antioxidant effect on the mitochondrial membranes lipid peroxidation model, better than the natural prototype and 2-ethyl-6-methylpyridin-3-ol with a related structure used in clinical practice.

Keywords Resveratrol · 2-stilbazole · 3-pyridinol · Antioxidant · DPPH · MDA

Introduction

Reactive oxygen species (ROS) are involved in the regulation of many physiological processes, performing critical functions in several cellular signaling pathways (Sies et al. 2017). At the same time, the cells have an antioxidant system as a protective mechanism that maintains the ROS concentration at a safe level, eliminating their oversupply if necessary. It is established that the imbalance between the ROS production and the antioxidant system ability to absorb them leads to oxidative stress, which contributes to the progression of age-related neurodegenerative diseases, diabetes and its complications, some types of cancers, and other serious pathologies (Pisoschi and Pop 2015). In this regard, antioxidant therapy through natural and synthetic exogenous antioxidants is a promising strategy for controlling the ROS overproduction.

The natural phytoalexin trans-resveratrol (**TR**) has a wide range of physiological activity, largely based on its antioxidant properties (Gülçin 2010). Numerous studies have shown that resveratrol has not only antioxidant but also cardioprotective (Bonnefont-Rousselot 2016), antitumor (Khan et al. 2016), neuroprotective (Singh et al. 2013), and anti-inflammatory properties (Poulsen et al. 2015), as well as the ability to influence aging (Markus and Morris 2008; Westphal et al. 2007). Nevertheless, the resveratrol usage in therapy is limited by its poor solubility in water, which leads to low bioavailability, as well as, low chemical stability (Berman et al. 2017). To solve this problem, various modifications of the native structure were proposed, including both transformations in functional groups and changes in the stilbene skeleton (Li et al. 2019). In particular, we previously reported on the synthesis of resveratrol analogs (**1a–e**) containing a 3-hydroxypyridine fragment and the radical scavenging activity detected for them (Semenov et al. 2018).

To continue this research, we synthesized a series of new derivatives (**2a–e**) in which the trans-resveratrol skeleton is combined with the fragment of 2-ethyl-6-methylpyridin-3-ol, because its chemical structure is similar to pyridoxine, which is positioned as an antihypoxant and antioxidant and used in clinical practice as hydrochloride (emoxypine) or succinate (mexidol) (Chesnokova et al. 2015) (Fig. 1).

Supplementary information The online version of this article (https://doi.org/10.1007/s00044-020-02585-6) contains supplementary material, which is available to authorized users.

✉ Alexander V. Semenov
salexan@mail.ru

[1] Department of Organic Chemistry, Physics and Chemistry Institute, National Research Mordovia State University, 68 Bolshevistskaya Str., Saransk 430005, Russia

[2] Medicine Institute, National Research Mordovia State University, 68 Bolshevistskaya Str., Saransk 430005, Russia

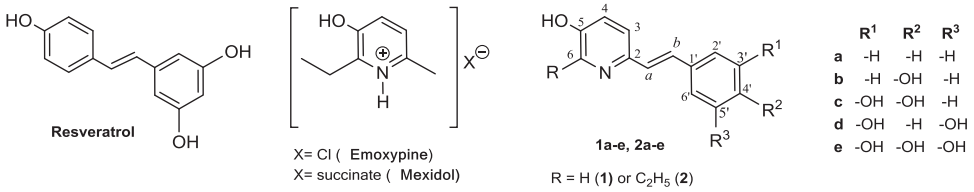

Fig. 1 Structures of resveratrol, emoxypine, mexidol and analogs **(1)** and **(2)**

The introduction of ethyl group in position 6 creates the steric shielding of the hydroxyl group, which should help to stabilize the phenoxyl radical and thereby increase the radical scavenging and antioxidant activity of the studied compounds.

In addition, we evaluated the antioxidant properties of all synthesized compounds in a model of induced oxidative damage to mitochondrial lipid membranes. It should be noted that it is mitochondria that play one of the key roles in the development of oxidative stress. The mitochondria respiratory chain is the main source of superoxide radicals, and the overproduction of superoxide in combination with a weakening of the antioxidant defense system leads to lipid peroxidation (LPO), primarily of the mitochondria and then of other cell structures (Bhatti et al. 2017; Indo et al. 2015; Ray et al. 2012). The mitochondrial damage severity largely determines the cell's life path. The massive mitochondria and cell structures damage leads to necrosis; with less severe damage, cell apoptosis can be initiated. The association of mitochondrial dysfunction with the overproduction of superoxide radicals as a universal mechanism of pathogenesis with the development of many diseases, in particular neurodegenerative, cardiovascular, inflammatory diseases, diabetes, and, in general, age-related pathology has been established. In this regard, mitochondria are an important object for the targeted study of antioxidant drugs, including resveratrol (Jardim et al. 2018).

Materials and methods

Experimental

Except where indicated, materials and reagents were used as supplied by the suppliers without further purification. The ^{1}H and ^{13}C NMR spectra were recorded on a Jeol JNM-ECX400 device (399.78 and 100.53 MHz, respectively) in DMSO-d_6 or $CDCl_3$. Chemical shifts were measured with reference to the residual protons of the solvents (DMSO-d_6, ^{1}H, 2.49 ppm, ^{13}C, 39.50 ppm; $CDCl_3$ ^{1}H, 7.25 ppm, ^{13}C, 77.00 ppm). Optical density measurements were carried out in the visible region at 517 nm on the "Shimadzu UV2600 Vis" instrument, the thickness of the absorbing layer was 10 mm. ESI-MS spectra were obtained on a Thermo Scientific MSQ Plus mass spectrometer in positive (negative) ion detection mode (source temperature 350 °C, gas-nebulizer−nitrogen, gas flow 50 l/min, needle voltage 4.5 kV, the voltage on cone 75 V, scanning in the range of 100−400 Da with a speed of 2 scans/s). The eluent is a mixture of ACN and 0.1% formic acid in a ratio of 60:40, a flow rate of 0.05 ml/min. Elemental analyses were performed on a vario MICRO cube (CHNS) unit. Microwave syntheses were carried out in the Monowave 300 reactor in special tightly sealed ampoules made of borosilicate glass.

Synthesis

2-Ethyl-3-methoxy-6-methylpyridine (3)

To 2-ethyl-3-hydroxy-6-methylpyridine suspension (3.00 g, 21.9 mmol) in ethanol (7 ml) cooled to 0 °C, the diazomethane (an 8-fold molar excess in diethyl ether solution, cooled) was added portion-wise at intervals of 24 h. After diazomethane addition the mixture was stirred for 1 h at 0 °C and then left at room temperature. Before adding a new portion of diazomethane the mixture was again cooled to 0 °C, then the procedure was repeated as described above. The solvent was removed, the residue was diluted with water, and the product was extracted with methyl tert-butyl ether. The extract was dried over anhydrous magnesium sulfate. After removing the solvent, the resulting product was purified by vacuum distillation. Colorless oil was obtained (2.50 g (76%), bp 75–80 °C/10–12 mmHg). ^{1}H NMR ($CDCl_3$, 400 MHz): δ 1.19 (*t*, $J = 7.6$ Hz, 3H); 2.44 (*s*, 3H), 2.79 (*q*, $J = 7.6$ Hz, 2H), 3.76 (*s*, 3H), 6.89 (*d*, $J =$ 8.3 Hz, 1H), 6.97 (d, $J = 8.3$ Hz, 1H). ^{13}C NMR ($CDCl_3$, 100 MHz): δ 13.0 (CH_3), 23.2 (CH_2), 26.0 (CH_3), 55.3 (CH_3, OCH_3), 117.5 (CH, C-4), 120.8 (CH, C-3), 148.4 (C, C-2), 151.2 (C, C-6), 152.5 (C, C-5); Anal. Calcd. for $C_9H_{13}NO$ (151.21): C 71.49, H 8.67, N 9.26; found: C 71.40, H 8.83, N 9.18.

1,6-Dimethyl-2-ethyl-3-methoxypyridinium iodide (4)

The compound (**3**) (1.00 g, 6.6 mmol) in chloroform solution (3 ml) was placed in a vial for the microwave reactor and methyl iodide (0.92 ml, 14.7 mmol) was added. The mixture was heated at 90 °C for 2 h, then the ampoule was cooled, the solvent was evaporated on a rotary evaporator. The resulting crystals were washed with ethyl acetate and dried in air.

Cream solid (1.75 g, 90%); mp 130–131 °C; ^{1}H NMR ($CDCl_3$, 400 MHz): δ 1.21 (*t*, $J = 7.8$ Hz, 3H), 2.79 (*s*, 3H), 3.12 (*q*, $J = 7.8$ Hz, 2H), 3.96 (*s*, 3H), 4.24 (*s*, 3H), 7.74 (*d*, $J = 8.7$ Hz, 1H), 7.95 (*d*, $J = 9.2$ Hz, 1H). ^{13}C NMR ($CDCl_3$, 100 MHz): δ 11.1 (CH_3), 21.3 (CH_2), 22.2 (CH_3), 42.2 (CH_3, NCH_3), 57.6 (CH_3, OCH_3), 125.8 (CH, C-4), 127.8 (CH, C-3), 145.9 (C, C-2), 150.8 (C, C-6), 154.3 (C, C-5); Anal. Calcd. for $C_{10}H_{16}INO$ (293.15): C 40.97, H 5.50, N 4.78; found: C 40.79, H 5.63, N 4.59.

General procedure for the condensation of the salt (4) with aromatic aldehydes

The reaction was carried out according to the method proposed by us in (Semenov et al. 2018) with some modifications. A solution of salt (**4**) (400 mg, 1.37 mmol), the corresponding aldehyde (1.37 mmol) and piperidine (0.135 ml) in a mixture of toluene (5 ml) and butanol-1 (1 ml) was boiled for 2 h. After cooling the mixture, precipitated solid products were filtered off, washed with diethyl ether, and dried in air.

(E)-2-ethyl-3-methoxy-1-methyl-6-styrylpyridin-1-ium iodide (5a) Light-yellow solid (350 mg, 67%); mp 210–211 °C (decomp.); ^{1}H NMR (DMSO-d_6, 400 MHz): δ 1.20 (3H, *t*, $J = 7.3$ Hz, CH_3), 3.14 (2H, *q*, $J = 7.3$ Hz, CH_2), 4.05 (3H, *s*, OCH_3), 4.27 (3H, *s*, NCH_3), 7.40–7.50 (3H, *m*, H-3′, H-4′, H-5′), 7.59 (2H, *s*, H-a, H-b), 7.80 (2H, *dd*, $J = 8.0$ Hz, $J = 1.2$ Hz, H-2′, H-6′), 8.20 (1H, *d*, $J = 9.2$ Hz, H-4), 8.27 (1H, *d*, $J = 9.2$ Hz, H-3); ^{13}C NMR (DMSO-d_6, 100 MHz): δ 10.8 (CH_3), 20.5 (CH_2), 41.3 (CH_3, NCH_3), 57.7 (CH_3, OCH_3), 118.9 (CH, C-a), 124.1 (CH, C-3), 125.8 (CH, C-4), 127.9 (2CH, C-2′, C-6′), 128.8 (2CH, C-3′, C-5′), 129.7 (CH, C-4′), 135.2 (C, C-1′), 139,6 (CH, C-b), 145.2 (C, C-2), 149.8 (C, C-6), 154.2 (C, C-5); MS (ESI) *m/z* calculated for $[C_{17}H_{20}NO^+] = 254.15$ (100.0%), 255.16 (18.4%) found 254.08 (100.0%), 255.09 (18.3%); Anal. Calcd. for $C_{17}H_{20}INO$ (381.26): C 53.56, H 5.29, N 3.67; found: C 53.44, H 5.32, N 3.61.

(E)-2-ethyl-3-methoxy-6-(4-methoxystyryl)-1-methylpyridin-1-ium iodide (5b) Yellow solid (430 mg, 77%); mp 211–213 °C (decomp.); ^{1}H NMR (DMSO-d_6, 400 MHz): δ 1.19 (3H, *t*, $J = 7.3$ Hz, CH_3), 3.12 (2H, *q*, $J = 7.3$ Hz, CH_2), 3.81 (3H, *s*, OCH_3), 4.04 (3H, *s*, OCH_3), 4.24 (3H, *s*, NCH_3), 7.02 (2H, *d*, $J = 8.7$ Hz, H-3′, H-5′), 7.41 (1H, *d*, $J = 16.0$ Hz, H-a), 7.55 (1H, *d*, $J = 16.0$ Hz, H-b), 7.76 (2H, *d*, $J = 8.7$ Hz, H-2′, H-6′), 8.18 (1H, *d*, $J = 9.6$ Hz, H-4), 8.24 (1H, *d*, $J = 9.6$ Hz, H-3); ^{13}C NMR (DMSO-d_6, 100 MHz): δ10.8 (CH_3), 20.4(CH_2), 41.1 (CH_3, NCH_3), 55.3 (CH_3, OCH_3), 57.6 (CH_3, OCH_3), 114.2 (2CH, C-3′, C-5′), 116.2 (CH, C-a), 123.6 (CH, C-3), 125.8 (CH, C-4), 127.8 (C, C-1′), 129.7 (2CH, C-2′, C-6′), 139.5 (CH, C-b), 145.6 (C,C-2), 149.4 (C, C-6), 153.8 (C, C-5), 160.6 (C, C-4′); MS (ESI) *m/z* calculated for $[C_{18}H_{22}NO_2^+] = 284.16$ (100.0%), 285.17 (19.5%) found 284.12 (100.0%), 285.15 (19.7%); Anal. Calcd. for $C_{18}H_{22}INO_2$ (411.28): C 52.57, H 5.39, N 3.41; found: C 52.43, H 5.50, N 3.37.

(E)-6-(3,4-dimethoxystyryl)-2-ethyl-3-methoxy-1-methylpyridin-1-ium iodide (5c) Yellow solid (430 mg, 72%); mp 197–198 °C; ^{1}H NMR (DMSO-d_6, 400 MHz): δ 1.19 (3H, *t*, $J = 7.3$ Hz, CH_3), 3.12 (2H, *q*, $J = 7.3$ Hz, CH_2), 3.81 (3H, *s*, OCH_3), 3.85 (3H, *s*, OCH_3), 4.04 (3H, *s*, OCH_3), 4.27 (3H, *s*, NCH_3), 7.02 (1H, *d*, $J = 8.1$ Hz, H-6′), 7.32 (1H, *d*, $J = 8.1$ Hz, H-5′), 7.44 (1H, *s*, H-2′), 7.45 (1H, *d*, $J = 16.0$ Hz, H-a), 7.54 (1H, *d*, $J = 16.0$ Hz, H-b), 8.17 (1H, *d*, $J = 9.2$, H-4), 8.23 (1H, d, $J = 9.2$ Hz, H-3); ^{13}C NMR (DMSO-d_6, 100 MHz): δ 10.8 (CH_3), 20.4(CH_2), 41.2 (CH_3, NCH_3), 55.6 (CH_3, OCH_3), 55.8 (CH_3, OCH_3), 57.6 (CH_3, OCH_3), 110.4 (CH, C-5′), 111.7 (CH, C-2′), 116.3 (CH, C-a), 122.5 (CH, C-6′), 123.6 (CH, C-3), 125.8 (CH, C-4), 128.1 (C, C-1′), 139.9 (CH, C-b), 145.7 (C, C-2), 148.9 (CH, C-6), 149.3 (C, C-3′), 150.5 (C, C-4′), 153.7 (C, C-5); MS (ESI) *m/z* calculated for $[C_{19}H_{24}NO_3^+] = 314.18$ (100.0%), 315.18 (20.5%) found 314.16 (100.0%), 315.15 (20.3%); Anal. Calcd. for $C_{19}H_{24}INO_3$ (441.31): C 51.71, H 5.48, N 3.17; found: C 51.63, H 5.55, N 3.04.

(E)-6-(3,5-dimethoxystyryl)-2-ethyl-3-methoxy-1-methylpyridin-1-ium iodide (5d) Light-yellow solid (240 mg, 40 %); mp 185–186 °C; ^{1}H NMR (DMSO-d_6, 400 MHz):δ 1.20 (3H, *t*, $J = 7.6$ Hz, CH_3), 3.14 (2H, *q*, $J = 7.3$ Hz, CH_2), 3.81 (6H, *s*, $2OCH_3$), 4.05 (3H, *s*, OCH_3), 4.26 (3H, *s*, NCH_3), 6.55 (1H, *t*, $J = 2.1$ Hz, H-4′), 6.97 (2H, *d*, $J = 2.1$ Hz, H-2′, H-6′), 7.49 (1H, *d*, $J = 16.0$ Hz, H-a), 7.58 (1H, *d*, $J = 16.0$ Hz, H-b), 8.19 (1H, *d*, $J = 9.3$ Hz, H-4), 8.23 (1H, *d*, $J = 9.3$ Hz, H-3); ^{13}C NMR (DMSO-d_6, 100 MHz): δ 10.8 (CH_3), 20.5 (CH_2), 41.3 (CH_3, NCH_3), 55.4 (CH_3, $2OCH_3$), 57.7 (CH_3, OCH_3), 101.8 (CH, C-4′), 106.1 (2CH, C-2′, C-6′), 119.5 (CH, C-a), 124.1 (CH, C-3), 125.8 (CH, C-4), 137.1 (CH, C-6), 139.7 (C, C-1′), 145.1 (CH, C-2), 150.0 (C, C-6), 154.3 (C, C-5), 160.7 (2C, C-3′, C-5′); MS (ESI) *m/z* calculated for $[C_{19}H_{24}NO_3^+] = 314.18$ (100.0%), 315.18 (20.5%) found 314.16 (100.0%), 315.16 (20.7%); Anal. Calcd. for $C_{19}H_{24}INO_3$ (441.31): C 51.71, H 5.48, N 3.17; found: C 51.65, H 5.59, N 3.09.

(E)-2-ethyl-3-methoxy-1-methyl-6-(3,4,5-trimethoxystyryl) pyridine-1-ium iodide (5e) Yellow solid (300 mg, 48%); mp 194–195 °C; ^{1}H NMR (DMSO-d_6, 400 MHz): δ 1.20 (3H, *t*, $J = 7.5$ Hz, CH_3), 3.14 (2H, *q*, $J = 7.5$ Hz, CH_2), 3.71 (3H, *s*, OCH_3), 3.86 (6H, *s*, $2OCH_3$), 4.05 (3H, *s*, OCH_3), 4.28 (3H, *s*, NCH_3), 7.14 (2H, *s*, H-2′, H-6′), 7.53 (2H, s, H-a, H-b), 8.21 (2H, *s*, H-4, H-3); ^{13}C NMR (DMSO-d_6, 100 MHz): δ 10.8 (CH_3), 20.5 (CH_2), 41.4

(CH_3, NCH_3), 56.2 ($2CH_3$, $2OCH_3$), 57.7 (CH_3, OCH_3), 60.1 (CH_3, OCH_3), 105.8 (2CH, C-2′, C-6′), 118.1 (CH, C-a), 123.9 (CH, C-3), 125.9 (CH, C-4), 130.8 (C, C-1′), 139.2 (CH, C-b), 139,9 (C, C-4′), 145.4 (C, C-2), 149.7 (CH, C-6), 153.0 (2C, C-3′, C-5′), 154.1 (C, C-5); MS (ESI) *m/z* calculated for $[C_{20}H_{26}NO_4^+] = 344.19$ (100.0%), 345.19 (21.6%) found 344.17 (100.0%), 345.18 (21.4%); Anal. Calcd. for $C_{20}H_{26}INO_4$ (471.34): C 50.97, H 5.56, N 2.97; found: C 50.84, H 5.61, N 2.90.

General procedure for the demethylation of salts (5a–e)

The procedure was carried out according to the method described in (Semenov et al. 2018). The obtained solid products were chromatographically purified on a column filled with silica gel, eluting with a mixture of methylene chloride and methanol (60:1–15:1).

(E)-2-ethyl-6-styrylpyridin-3-ol (2a) White solid (105 mg, 60%); mp 185–186 °C; ^{1}H NMR (DMSO-d_6, 400 MHz): δ 1.21 (3H, *t*, $J = 7.6$ Hz, CH_3), 2.74 (2H, *q*, $J = 7.6$ Hz, CH_2), 7.07–7.27 (4H, *m*, H-3, H-4, H-a, H-4′), 7.32–7.41 (3H, *m*, H-3′, H-5′, H-b), 7.57 (2H, *d*, $J = 7.3$ Hz, H-2′, H-6′), 9.79 (1H, *s*, OH); ^{13}C NMR (DMSO-d_6, 100 MHz):δ 12.2 (CH_3), 25.2 (CH_2) 120.7 (CH, H-3), 121.4 (CH, C-4), 126.4 (2CH, C-2′, C-6′), 127.3 (CH, C-a), 128.1 (CH, C-4′), 128.4 (CH, C-b), 128.6 (2CH, C-3′, C-5′), 136.9 (C, C-1′), 145.1 (CH, C-6), 150.1 (C, C-2), 150.4 (C, C-5); MS (ESI) *m/z* calculated for $[C_{15}H_{15}NO+H^+] = 226.12$ (100.0%), 227.13 (16.2%), found 226.11 (100.0%), 227.11 (16.2%); calculated for $[C_{15}H_{15}NO-H^+] = 224.11$ (100.0%), 225.11 (16.2%) found 224.07 (100.0%), 225.07 (16.1%); Anal. Calcd. for $C_{15}H_{15}NO$ (225.29): C 79.97, H 6.71, N 6.22; found: C 79.82, H 6.85, N 6.09.

(E)-2-ethyl-6-(4-hydroxystyryl)pyridin-3-ol (2b) Yellow solid (94 mg, 50%); mp 213–214 °C; ^{1}H NMR (DMSO-d_6, 400 MHz): δ 1.21 (3H, *t*, $J = 7.3$ Hz, CH_3), 2.74 (2H, *q*, $J = 7.6$ Hz, CH_2), 6.77 (2H, *d*, $J = 8.7$ Hz, H-3′, H-5′), 6.93 (1H, *d*, $J = 16.0$ Hz, H-b), 7.07 (1H, *d*, $J = 8.2$ Hz, H-3), 7.15 (1H, *d*, $J = 8.7$ Hz, H-4), 7.28 (H, *d*, $J = 16.0$ Hz, H-a), 7.40 (2H, *d*, $J = 8.7$ Hz, H-2, H-6), 9.60 (2H, br *s*, OH-Ph, OH-Py); ^{13}C NMR (DMSO-d_6, 100 MHz): δ 12.3 (CH_3), 25.2 (CH_2), 115.5 (2CH, C-3′, C-5′), 119.9 (CH, C-3), 121.6 (CH, C-4), 125.2 (CH, C-a), 127.8 (2CH, C-2′, C-6′), 128.1 (C, C-1′), 128.3 (CH, C-b), 145.8 (CH, C-6), 149.6 (C, C-2), 150.2 (C, C-5), 157.2 (C, C-4′); MS (ESI) *m/z* calculated for $[C_{15}H_{15}NO_2+H^+] = 242.12$ (100.0%), 243.12 (16.2%), found 242.14 (100.0%), 243.14 (16.7%); calculated for $[C_{13}H_{11}NO_2-H^+] = 240.10$ (100.0%), 241.11 (16.2%) found 240.08 (100.0%), 241.07 (16.3%); Anal. Calcd. for $C_{15}H_{15}NO_2$ (241.29): C 74.67, H 6.27, N 5.81; found: C 74.53, H 6.32, N 5.75.

(E)-4-(2-(6-ethyl-5-hydroxypyridin-2-yl)vinyl)benzene-1,2-diol (2c) Yellow solid (100 mg, 50%); mp 141–143 °C; ^{1}H NMR (DMSO-d_6, 400 MHz): δ 1.20 (3H, *t*, $J = 7.6$ Hz, CH_3), 2.72 (2H, *q*, $J = 7.6$ Hz, CH_2), 6.72 (1H, *d*, $J = 8.3$ Hz, H-4′), 6.81–6.85 (2H, *m*, H-6′, H-b), 6.97 (1H, *d*, $J = 2.3$ Hz, H-2′), 7.06 (1H, *d*, $J = 8.2$ Hz, H-3), 7.15 (1H, *d*, $J = 8.3$ Hz, H-4), 7.20 (1H, *d*, $J = 16.0$ Hz, H-a), 9.34 (3H, br *s*, 2OH-Ph, OH-Py); ^{13}C NMR (DMSO-d_6, 100 MHz): δ 12.3 (CH_3), 25.2(CH_2), 113.2 (CH, C-2′), 115.7 (CH, C-5′), 118.6 (CH, C-6′), 120.0 (CH, C-3), 121.6 (CH, C-4), 125.1 (CH, C-a), 128.6 (CH, C-b), 128.7 (C, C-1′), 145.4 (CH, C-6), 145.5 (C, C-3′), 145.8 (C, C-4′), 149.6 (C, C-2), 150.2 (C, C-5); MS (ESI) *m/z* calculated for $[C_{15}H_{15}NO_3+H^+] = 258.11$ (100.0%), 259.12 (16.2%) found 258.08 (100.0%), 259.10 (16.5 %); calculated for $[C_{13}H_{11}NO_3-H^+] = 256.10$ (100.0%), 257.10 (16.2%) found 256.08 (100.0%), 257.09 (16.3%); Anal. Calcd. for $C_{15}H_{15}NO_3$ (257.29): C 70.02, H 5.88, N 5.44; found: C 69.93, H 5.97, N 5.38.

(E)-5-(2-(6-ethyl-5-hydroxypyridin-2-yl)vinyl)benzene-1,3-diol (2d) Cream solid (94 mg, 47%); mp 157–159 °C; ^{1}H NMR (DMSO-d_6, 400 MHz): δ 1.20 (3H, *t*, $J = 7.6$ Hz, CH_3), 2.72 (2H, *q*, $J = 7.6$ Hz, CH_2), 6.14 (1H, *t*, $J = 2.0$ Hz, H-4′), 6.41 (2H, *d*, $J = 2.0$ Hz, H-2′, H-6′), 6.92 (1H, *d*, $J = 16.1$ Hz, H-b), 7.07 (1H, *d*, $J = 8.3$ Hz, H-3), 7.16 (1H, *d*, $J = 16.1$ Hz, H-a), 7.21 (1H, *d*, $J = 7.8$ Hz, H-4), 9.18 (2H, br *s*, 2OH-Ph), 9.76 (1H, br *s*, OH-Py); ^{13}C NMR (DMSO-d_6, 100 MHz): δ 12.2 (CH_3), 25.1 (CH_2), 102.2 (CH, C-4′), 104.6 (2CH, C-2′, C-6′), 120.6 (CH, C-3), 121.5 (CH, C-4), 127.8 (CH, C-a), 128.8 (CH, C-b), 138.6 (CH, C-1′), 145.1 (C, C-6), 150.0 (C, C-2), 150.3 (C, C-5), 158.5 (2C, C-3′, C-5′); MS (ESI) *m/z* calculated for $[C_{15}H_{15}NO_3+H^+] = 258.11$ (100.0%), 259.12 (16.2%) found 258.10 (100.0%), 259.11 (16.5%); calculated for $[C_{15}H_{15}NO_3-H^+] = 256.10$ (100.0%), 257.10 (16.2%) found 256.09 (100.0%), 257.10 (16.1%); Anal. Calcd. for $C_{15}H_{15}NO_3$ (257.29): C 70.02, H 5.88, N 5.44; found: C 69.90, H 5.95, N 5.36.

(E)-5-(2-(6-ethyl-5-hydroxypyridin-2-yl)vinyl)benzene-1,2,3-triol (2e) Orange solid (85 mg, 40%); mp 168–170 °C (decomp.); ^{1}H NMR (DMSO-d_6, 400 MHz): δ 1.19 (3H, *t*, $J = 7.6$ Hz, CH_3), 2.71 (2H, *q*, $J = 7.6$ Hz, CH_2), 6.49 (2H, *s*, H-2′, H-6′), 6.55 (1H, *d*, $J = 16.1$ Hz, H-b), 7.05 (1H, *d*, $J = 8.3$ Hz, H-3), 7.09 (1H, *d*, $J = 16.1$ Hz, H-a), 7.15 (1H, *d*, $J = 8.3$ Hz, H-4), 8.22 (1H, br *s*, OH-Ph), 8.81 (2H, br *s*, 2OH-Ph), 9.64 (1H, br *s*, OH-Py); ^{13}C NMR (DMSO-d_6, 100 MHz): δ 12.2 (CH_3), 25.1 (CH_2), 105.6 (2CH, C-2′, C-6′), 119.9 (CH, C-3), 121.5 (CH, C-a), 125.2 (CH, C-4), 127.6 (CH, C-1′), 129.0 (C, C-b), 133.4 (C, C-4′), 145.7 (CH, C-6), 146.1 (2C, C-3′, C-5′), 149.6 (C, C-2), 150.1 (C, C-5); MS (ESI) *m/z* calculated for $[C_{15}H_{15}NO_4+H^+] = 274.11$ (100.0%), 275.11 (16.2%) found 274.09 (100.0%),

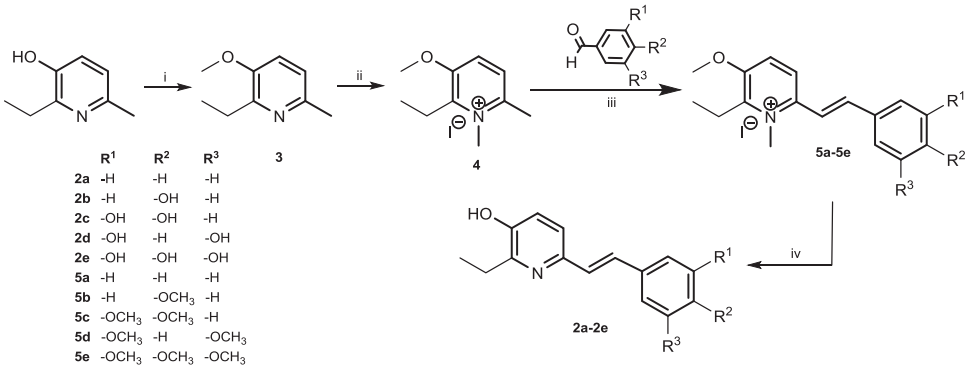

Scheme 1 General synthetic route for the synthesis of the resveratrol analogs **2a**–**2e**. Reagents and conditions: (i) CH_2N_2, diethyl ether; (ii) CH_3I, $CHCl_3$, MW; (iii) butanol-toluene, piperidine; (iv) Py·HCl

275.10 (16.5%); calculated for $[C_{15}H_{15}NO_4-H^+] = 272.09$ (100.0%), 273.10 (16.2%) found 272.09 (100.0%), 273.09 (16.3%); Anal. Calcd. for $C_{15}H_{15}NO_4$ (273.29): C 65.92, H 5.53, N 5.13; found: C 65.80, H 5.68, N 4.91.

Isolation of liver mitochondria

Liver mitochondria were isolated on white mongrel male mice aged 3 months. Typically, the isolation medium for mitochondria consists of a buffer solution containing isosmotic sucrose and/or mannitol; however, it should be borne in mind that such solutions are neither isotonic nor physiological and can induce abnormal ions and water fluxes across the membranes of mitochondria altering the composition of the matrix. At the same time, a study (Corcelli et al. 2010) showed that mitochondria isolated in KCl buffer are coupled and able to maintain a stable transmembrane charge separation. As a result, in our work, as a selection medium, we used phosphate-buffered saline (PBS), pH 7.4 (137 mM NaCl, 2.7 mM KCl, 10 mM Na_2HPO_4, 2 mM KH_2PO_4). All manipulations were carried out at 4 °C.

The extracted liver was washed with cooled PBS and homogenized in the same buffer (10% w/v) for 15 s at intervals of 1 min in a Potter-Elvehjem homogenizer. The resulting homogenate was centrifuged at 600 g for 10 min to remove nuclei and cell debris. The resulting supernatant fractions were centrifuged twice at 8000 g for 10 min and the pellet was resuspended in 0.5 ml of PBS. After measuring the protein concentration by the Bradford method (He 2011), the final mitochondrial suspensions were used for 2 h to evaluate Fe^{2+}/ascorbate-induced LPO.

MDA product measurement

Fe^{2+}/ascorbate-induced MDA levels were determined in liver mitochondria (Devasagayam et al. 1983). The formation of MDA due to the formation of substances reacting with thiobarbituric acid (TBARS) was used to monitor LPO. A mitochondrial suspension was incubated at 37 °C in 0.1 M PBS (pH 7.4) and adjusted to a final protein concentration of 1 mg/ml. Mitochondria with the studied substances (at final concentrations of 3, 7, 11, 15, 20, and 40 μM) were incubated for 30 min, after which LPO was initiated by Fe^{2+} (20 μM)/ascorbate (100 μM) and incubated for another 30 min at 37 °C. At the end of the incubation time, 0.02% w/v BHT was added to inhibit LPO (this amount of BHT completely prevents the formation of any non-specific TBARS), after which TCA-TBA-HCl (15% w/v trichloroacetic acid (TCA); 0.375% w/v TBA; 0.25 M HCl) was added. The resulting mixture was heated at 80 °C for 30 min. After cooling, the precipitate was removed by centrifugation. The MDA in the supernatant was determined at 532 nm using an extinction coefficient of 1.56×10^5.

Data for each analyzed value were obtained in triplicate or more. Statistical processing of the results was carried out in the Microsoft Excel 2010 software package. Differences were considered statistically significant at $p < 0.05$.

Results and discussion

Chemistry

Synthesis of target compounds (**2**) was carried out according to our previously developed scheme (Semenov et al. 2018) (Scheme 1).

It should be noted that at the stage of intermediate (**4**) preparation we had to abandon the one-pot process, which in this case led to a contaminated product and required a chromatographic purification stage, which significantly reduced the yield. As a result, at first, we synthesized the compound (**3**) by methylation with diazomethane of the free base obtained from the 2-ethyl-3-hydroxy-6-methylpyridine hydrochloride substance (emoxypine), which was further quaternized with methyl iodide under microwave initiation conditions. The product (**4**) was further introduced into the condensation reaction with the corresponding aromatic aldehydes. At the same time, the replacement of butanol with the toluene–butanol system made it possible to facilitate the isolation and increase the yield and purity of the

obtained products (**5**). Their demethylation with anhydrous pyridinium chloride upon heating led to the target compounds (**2**). The structures of compounds (**5**) and (**2**), are convincingly confirmed by ^{1}H and ^{13}C NMR spectroscopy. In most cases, the E-configuration of the double bond is confirmed by the presence of characteristic doublet signals with coupling constants about 16 Hz in the ^{1}H NMR spectra. But the unambiguous assignment of signals for structures (**2a**) and (**5a**) is difficult due to their superposition. The ^{1}H NMR spectrum of compound (**5e**) is also non-standard, in which, contrary to expectations, only three singlet signals are recorded in the low-field part. Bearing in mind that sometimes coupling will lead to very complicated patterns as a result of the J values that vary widely due to the relationship between the hydrogens involved, we nevertheless postulate the E-configuration for the indicated structures by looking at the chemical shift and comparing with related structures. When alkenyl hydrogen atoms are not symmetrically substituted on a double-bonded carbon, the hydrogens of a cis and trans isomer will yield a different shift on the NMR spectrum. Because the coupling constant is smaller in a cis isomer than in a trans isomer, the NMR spectrums of the two isomers are different conveying the hydrogens in a cis isomer to be slightly more upfield to the right of the spectrum and trans hydrogens to be more downfield to the left. The spectra analysis of cis and trans isomers of unsubstituted 2-styrylpyridine (Wakabayashi et al. 1990) and related hydroxylated structures (Garipov et al. 2018) shows that the chemical shifts of olefin protons of cis isomers lie in the region of <7 ppm, and for trans isomers exceed this value.

Radical scavenging activity

The radical scavenging activity of the obtained compounds was evaluated using the DPPH test as described in (Semenov et al. 2018). Comparative data on IC_{50} values are given in Table 1 and Fig. 2.

The results analysis shows that in the case of derivatives **a** and **d**, the introduction of an ethyl fragment does lead to a significant increase in the radical scavenging activity, while in other cases this transformation does not significantly affect the IC_{50} value, and in the case of derivative **c**, it significantly increases. The reasons for such differences, in our opinion, should be sought in the structural features of these two groups of derivatives, namely, the hydroxyl group presence at position 4′ in structures **b**, **c**, and **e** of **a** and its absence in derivatives **a** and **d**. Due to these differences, the interaction of radical particles with compounds of the first group should lead to the formation of sufficiently stable semiquinoid anion-radical structures, which are more resistant to disproportionation and dimerization due to charge repulsion. Thus, in this case, the introduction of a donor ethyl group can have a destabilizing effect due to the ability to deprotonate decreasing. In addition, in the case of compounds **c** and **e**, the influence of neighboring hydroxyl groups due to the formation of intramolecular hydrogen bonds will be the most important stabilizing factor, which makes the hydroxyl group in the 4′ position more active. Under similar conditions, neutral phenoxyl radicals are generated from derivatives of the second group, the stabilization of which is significantly influenced by the presence of an ortho-alkyl substituent, which leads to the observed substantial activity increasing (Scheme 2).

Antioxidant activity on mitochondria

To evaluate the antioxidant properties of the studied compounds, we turned to the widely used Fe^{2+}/ascorbate system used to generate hydroxyl radicals in the induced LPO study. Mouse liver mitochondria were used as the object of study, and the LPO process was controlled by the formation of malondialdehyde (MDA). The object choice was determined by the key role of mitochondria in cell viability and regulation of its functions. In addition, data were obtained in some studies testify to the complex mechanisms of the antioxidant activity of many drugs in vivo, which are far

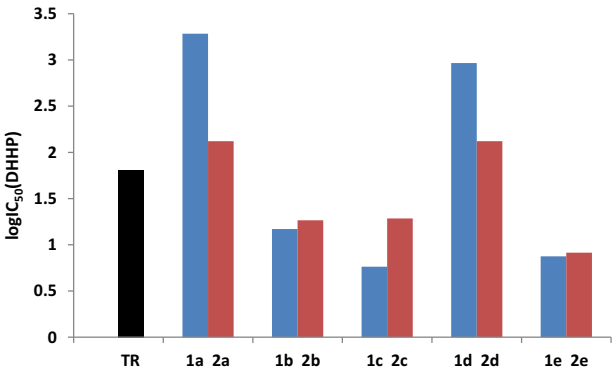

Fig. 2 The $logIC_{50}$ values (DPPH• test) of the analogs (**1**) and (**2**) in comparison with resveratrol

Table 1 The DPPH test IC_{50} values of the testing compounds and resveratrol

Compound	TR	1a	2a	1b	2b	1c	2c	1d	2d	1e	2e
IC_{50}, μM	64.5 ± 10[a]	1923 ± 57	132.10 ± 9.25	14.8 ± 1.50	18.40 ± 0.32	5.8 ± 0.30	19.26 ± 0.80	926 ± 18	132.18 ± 1.43	7.5 ± 0.59	8.21 ± 0.03
$logIC_{50}$	1.809	3.284	2.121	1.170	1.265	0.763	1.285	2.967	2.121	0.875	0.914

[a]62.5 ± 4.16 μM (Khanduja and Bhardwaj 2003); 74.0 ± 5.3 μM (Fauconneau et al. 1997)

Scheme 2 Proposed radical scavenging mechanisms

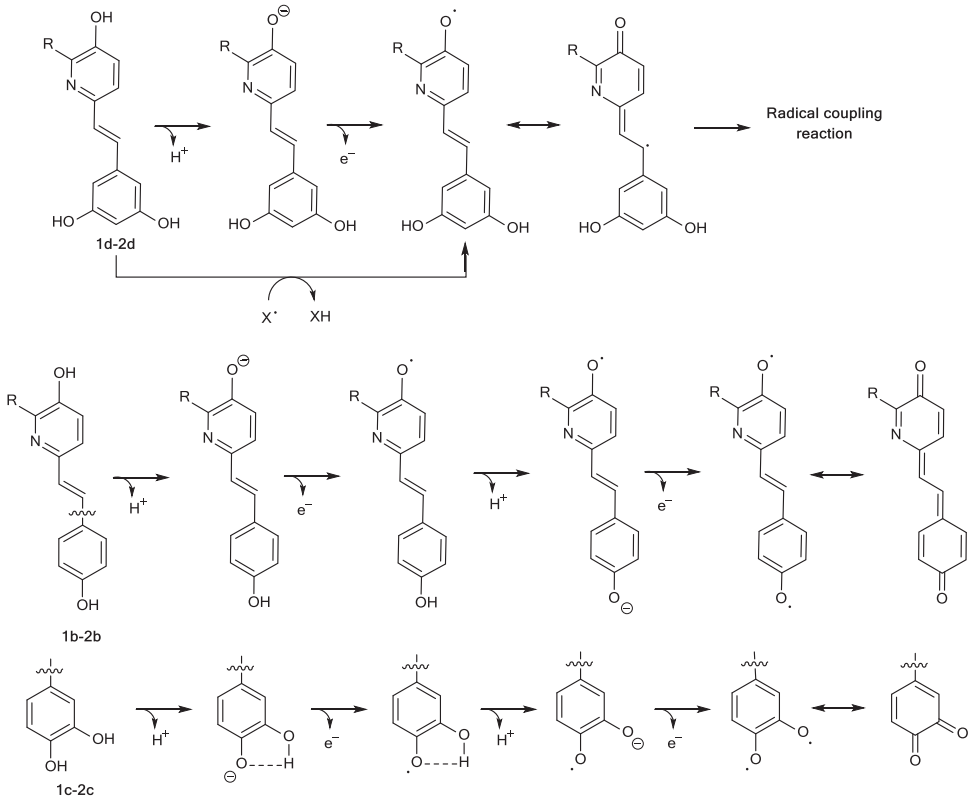

from being limited by the ability of substances to perform simply the function of a free radical trap. So, it was shown that some drugs that don't have antioxidant activity in vitro in standard tests for quenching free radical reactions exhibit high antioxidant activity in biological model systems, in particular in studies on mitochondria. The presence of antioxidant-binding sites in the hydrophobic core of the inner mitochondrial membrane or in the mitochondrial matrix is assumed. These sites can associate various unrelated hydrophobic compounds that modulate ROS-associated mitochondrial processes, regardless of activity to remove free radicals (Elimadi et al. 1998). The presence of such mechanisms can make a significant contribution to the resulting antioxidant effect of a substance. In addition, it is known that a suspension of mitochondria (in contrast to cell homogenate) can remain viable under adequate storage conditions throughout the experiment without adding chemicals that can distort the results of evaluating antioxidant properties; this allows getting the most reliable results. In this regard, to further determine the antioxidant properties mitochondria were chosen as a model system. The studies were carried out for a concentration range from 3 to 40 µm. Resveratrol and emoxypine, having a related structure, were taken as comparison compounds. The results of the studies are summarized in Fig. 3.

A comparison of the relative MDA concentrations in intact animals and control group animals suggests a statistically significant increase in the TBA concentration of sensitive products under the conditions of the LPO model, which indicates its validity.

In general, it should be noted that in all cases there is a fairly clear dependence of the decrease in the TBA production of sensitive compounds on the concentration of antioxidants introduced into the system. However, while the antioxidant activity of resveratrol and most of its studied synthetic analogs are already evident at low concentrations (3–7 µm), in the case of emoxipin and derivatives (**1d**) and (**1e**), a statistically significant MDA level decreasing begins to appear only at concentrations above 15 µm.

Based on the obtained data, antioxidant concentrations were calculated at which 50% inhibition of TBA generation of sensitive products occurs (Table 2 and Fig. 4). The maximum inhibitory activity is observed for compounds (**b**) and (**c**), which significantly reduce the MDA level, both in comparison with the control and in comparison with **TR** already at a concentration of 3 µm.

The relationship of the radical scavenging activity in the DPPH test with the data on antioxidant properties in the mitochondrial membranes LPO model was evaluated (Fig. 5).

It was found that when assessing correlation dependencies using a complete set of data (including **TR**), there is no statistically significant relationship between the studied parameters. However, analyzing the graph, one can see extremely large values of the parameters ("outliers" that fall outside the range of $M \pm 2\sigma$) related to compounds (**1e**) and (**2e**).

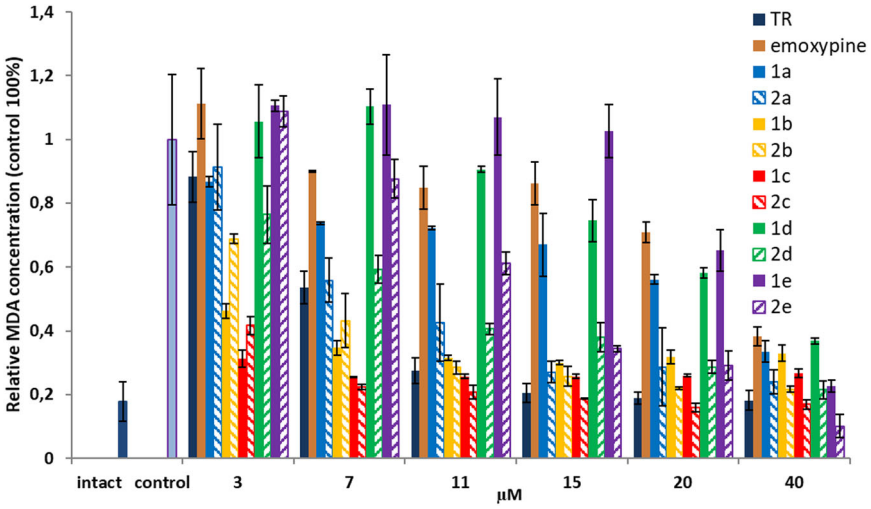

Fig. 3 Relative MDA content under different concentration of tested compounds

Table 2 The MDA test IC_{50} values of the testing compounds and resveratrol

Compound	TR	1a	2a	1b	2b	1c	2c	1d	2d	1e	2e
IC_{50}, μM	7.44 ± 0.52	23.92 ± 2.40	8.67 ± 1.40	2.69 ± 0.18	5.74 ± 0.45	1.90 ± 0.11	2.43 ± 0.17	23.42 ± 1.19	9.10 ± 0.45	25.58 ± 0.98	12.43 ± 0.64
logIC_{50}	0.872	1.379	0.938	0.430	0.759	0.279	0.386	1.370	0.959	1.408	1.094

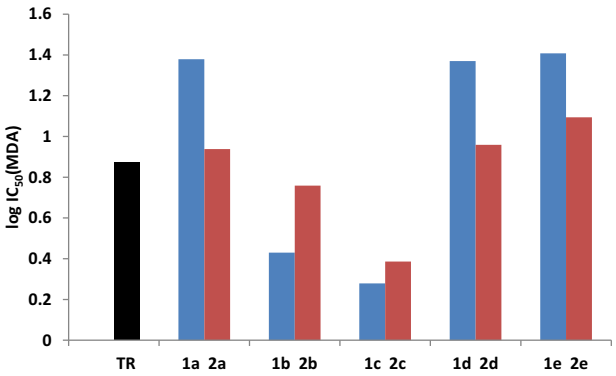

Fig. 4 The logIC_{50} values (MDA test) of the analogs (**1**) and (**2**) in comparison with resveratrol

In this regard, the data was "cleaned" and, as a result, a correlation between the studied values was revealed. Next, a correlation equation was constructed using a linear regression model, the relevance of which was evaluated by three criteria: the correlation coefficient (R), the determination coefficient (R^2), the value of the Fisher coefficient (F), and standard deviation (s)

$$\log IC_{50}(\mathrm{MDA}) = 0.455(\pm 0.049)\log IC_{50}(\mathrm{DHHP}) - 0.029(\pm 0.099),$$

$$n = 9;\ R = 0.96;\ R^2 = 0.92;\ s = 0.12;\ F = 85.68.$$

Thus, a statistically significant positive correlation between the data obtained in the DPPH test and the results of biological tests was confirmed.

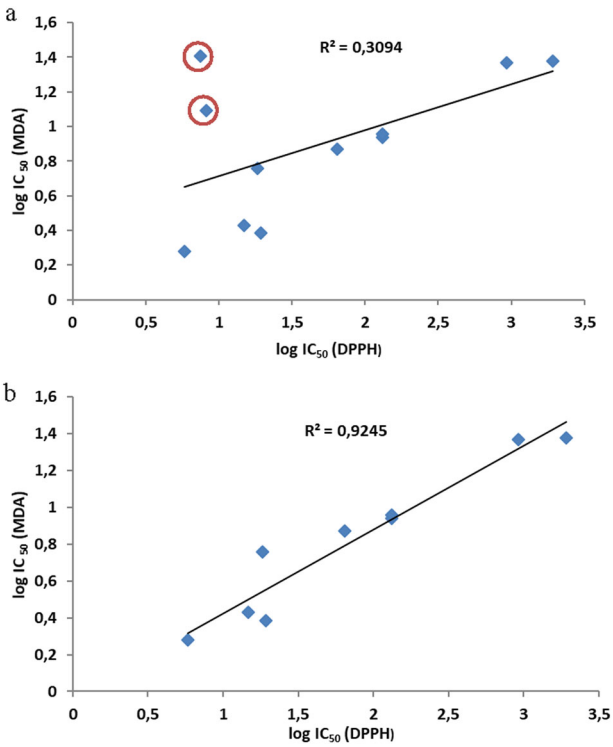

Fig. 5 Correlation between the radical scavenging activity and antioxidant properties for a complete set of testing compounds (**a**) and excluding pyrogallol derivatives (**b**)

The reasons for the significant difference in the behavior of structures (**1e**) and (**2e**) in the DPPH test and the biological system, apparently, should be sought in the parameters

Table 3 The predicted TPSA and logP values of the testing compounds and resveratrol

Compound	TR	1a	2a	1b	2b	1c	2c	1d	2d	1e	2e
TPSA, Å	60.69	33.12	33.12	53.35	53.35	73.58	73.58	73.58	73.58	93.81	93.81
logP	2.59	2.65	3.23	2.25	2.82	1.85	2.43	1.00	1.58	1.03	1.60

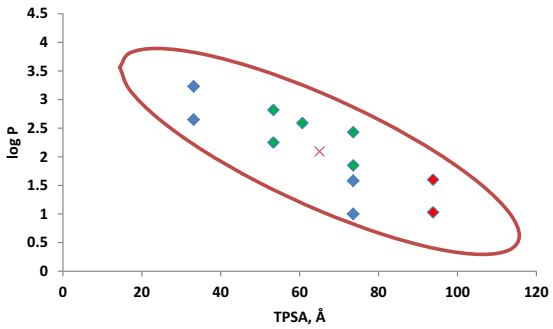

Fig. 6 Tested compounds plotted on TPSA – logP axes with a standard 95% confidence ellipse

of their bioavailability. The most important condition for the manifestation of biological activity is the ability of molecules to passively transport through cell membranes. The traditional parameter evaluating this property is the octanol-water partition coefficient (logP). Along with it, a useful parameter for assessing penetration is the polar surface area (PSA) defined as the sum of the surfaces of polar atoms in a molecule.

The combination of these descriptors within «Egan egg» model (Egan et al. 2000) is currently widely used to predict the intestinal absorption, Caco-2 monolayers penetration, and blood–brain barrier crossing (Daina and Zoete 2016). Moreover, a simpler and faster calculated topological PSA (TPSA) is often used instead of 3D PSA, because it was found that these descriptors are highly correlated and have almost identical values (Ertl et al. 2000).

We calculated logP and TPSA for the studied compounds using the ChemOffice software package, the results are presented in Table 3 and Fig. 6.

As can be seen from Fig. 6, compounds (**1e**) and (**2e**) having sufficiently high TPSA values and relatively low logP values, (red dots) are located on the periphery of the elliptical region, in the center of which are the compounds exhibiting the highest antioxidant activity (green dots). Thus, the presence of a large number of hydroxyl groups in derivatives (**1e**) and (**2e**) obviously complicates the transport through the cell lipid membrane. As a result the pronounced antioxidant effect for them appears only at a concentration of 40 µm. Indirect evidence of the relatively low ability to penetrate into the cells for compound (**1e**) can be seen in our previously obtained data on the fluorescence properties of compounds **1a–e** (Semenov et al. 2019).

In particular, it was found that during the treatment of fibroblasts with the studied compounds, their accumulation was observed inside the cells, which was recorded by fluorescence microscopy. Moreover, it was precisely for compound (**1e**) that the level of observed fluorescence was minimal, despite the comparable values of the quantum fluorescence yields obtained for the considered line of compounds in in vitro experiments.

Conclusion

The results obtained indicate that the introduction of a screening ethyl group at position 6 of the hydroxypyridine fragment has an ambiguous effect on the radical scavenging and antioxidant properties of the studied stilbazoles. A significant dependence of these properties on the nature of the hydroxylation of the benzene fragment is observed. The likely reason for the differences lies in the structural features of the resulting radical intermediates, which requires additional research. It was shown that the radical scavenging activity of the compounds manifested in DPPH tests in most cases satisfactorily correlates with their antioxidant activity studied in the model of Fe^{2+}/ascorbate-induced mitochondrial membranes LPO. However, in some examples, the ability of compounds to penetrate in the cell through simple transmembrane diffusion has a significant effect on the antioxidant activity shown, which also requires a more thorough study. As a result, a series of stilbazolic resveratrol analogs with pronounced radical scavenging and antioxidant properties was obtained that exceeded the natural prototype and used in clinical practice 2-ethyl-6-methylpyridin-3-ol with related structure.

Funding The reported study was funded by RFBR according to the research project No. 18-43-130004.

Compliance with ethical standards

Conflict of interest The authors declare that they have no conflict of interest.

Publisher's note Springer Nature remains neutral with regard to jurisdictional claims in published maps and institutional affiliations.

References

Berman AY, Motechin RA, Wiesenfeld MY, Holz MK (2017) The therapeutic potential of resveratrol: a review of clinical trials. NPJ Precis Oncol 1:35

Bhatti JS, Bhatti GK, Reddy PH (2017) Mitochondrial dysfunction and oxidative stress in metabolic disorders—a step towards

mitochondria based therapeutic strategies. Biochim Biophys Acta 1863:1066–1077

Bonnefont-Rousselot D (2016) Resveratrol and cardiovascular diseases. Nutrients 8:250–273

Chesnokova NB, Beznos OV, Pavlenko TA, Zabozlaev AA, Pavlova MV (2015) Effects of hydroxypyridine derivatives mexidol and emoxypin on the reparative processes in rabbit eye on the models of corneal epithelial defect and conjunctival ischemia. Bull Exp Biol Med 158:346–348

Corcelli A, Saponetti MS, Zaccagnino P, Lopalco P, Mastrodonato M, Liquori GE, Lorusso M (2010) Mitochondria isolated in nearly isotonic KCl buffer: focus on cardiolipin and organelle morphology. Biochim Biophys Acta 1798:681–687

Daina A, Zoete V (2016) A BOILED-Egg to predict gastrointestinal absorption and brain penetration of small molecules. ChemMedChem 11:1117–1121

Devasagayam TPA, Pushpendran CK, Eapen J (1983) Differences in lipid peroxidation of rat liver rough and smooth microsomes. Biochim Biophys Acta 750:91–97

Egan WJ, Merz Jr. KM, Baldwin JJ (2000) Prediction of drug absorption using multivariate statistics. J Med Chem 43:3867–3877

Elimadi A, Bouillot L, Sapena R, Tillement J-P, Morin D (1998) Dose-related inversion of cinnarizine and flunarizine effects on mitochondrial permeability transition. Eur J Pharm 348:115–121

Ertl P, Rohde B, Selzer P (2000) Fast calculation of molecular polar surface area as a sum of fragment-based contributions and its application to the prediction of drug transport properties. J Med Chem 43:3714–3717

Fauconneau B, Waffo-Teguo P, Huguet F, Barrier L, Decendit A, Merillon J-M (1997) Comparative study of radical scavenger and antioxidant properties of phenolic compounds from vitis vinifera cell cultures using in vitro tests. Life Sci 61:2103–2110

Garipov MR, Strelnik AD, Shtyrlin NV, Nagimova AI, Naumov AK, Morozov OA, Balakin KV, Shtyrlin YG (2018) Synthesis and nonlinear optical properties of pyridoxine-based stilbazole derivatives and their azo-analogs. Synth Commun 48:768–777

Gülçin I (2010) Antioxidant properties of resveratrol: a structure-activity insight. Innov Food Sci Emerg Technol 11:210–218

He F (2011) Bradford protein assay. Bio 101:e45

Indo HP, Yen H-C, Nakanishi I, Matsumoto K, Tamura M, Nagano Y, Matsui H, Gusev O, Cornette R, Okuda T, Minamiyama Y, Ichikawa H, Suenaga S, Oki M, Sato T, Ozawa T, Clair DKS, Majima HJ (2015) A mitochondrial superoxide theory for oxidative stress diseases and aging. J Clin Biochem Nutr 56:1–7

Jardim FR, de Rossi FT, Nascimento MX, da Silva Barros RG, Borges PA, Prescilio IC, de Oliveira MR (2018) Resveratrol and brain mitochondria: a review. Mol Neurobiol 55:2085–2101

Khan OS, Bhat AA, Krishnankutty R, Mohammad RM, Uddin S (2016) Therapeutic potential of resveratrol in lymphoid malignancies. Nutr Cancer 68:365–373

Khanduja KL, Bhardwaj A (2003) Stable free radical scavenging and antiperoxidative properties of resveratrol compared in vitro with some other bioflavonoids. Indian J Biochem Biophys 40:416–22

Li Q-S, Li Y, Deora GS, Ruan B-F (2019) Derivatives and analogues of resveratrol: recent advances in structural modification. Mini-Rev Medicinal Chem 19:809–825

Markus MA, Morris BJ (2008) Resveratrol in prevention and treatment of common clinical conditions of aging. Clin Inter Aging 3:331–339

Pisoschi AM, Pop A (2015) The role of antioxidants in the chemistry of oxidative stress: a review. Eur J Med Chem 97:55–74

Poulsen MM, Fjeldborg K, Ornstrup MJ, Kjær TN, Nøhr MK, Pedersen SB (2015) Resveratrol and inflammation: Challenges in translating pre-clinical findings to improved patient outcomes. Biochim Biophys Acta 1852:1124–1136

Ray PD, Huang B-W, Tsuji Y (2012) Reactive oxygen species (ROS) homeostasis and redox regulation in cellular signaling. Cell Signal 24:981–990

Semenov AV, Balakireva OI, Tarasova IV, Burtasov AA, Semenova EV, Petrov PS, Minaeva OV, Pyataev NA (2018) Synthesis, theoretical, and experimental study of radical scavenging activity of 3-pyridinol containing *trans*-resveratrol analogs. Med Chem Res 27:1298–1308

Semenov AV, Balakireva OI, Tarasova IV, Semenova EV, Minaeva OV (2019) Spectroscopic properties of some hydroxylated 2-stilbazole derivatives. J Fluoresc 29:1301–1309

Sies H, Berndt C, Jones DP (2017) Oxidative stress. Annu Rev Biochem 86:715–748

Singh N, Agrawal M, Doré S (2013) Neuroprotective properties and mechanisms of resveratrol in in vitro and in vivo experimental cerebral stroke models. ACS Chem Neurosci 4:1151–1162

Wakabayashi S, Kiyohara Y, Kameda S, Uenishi J, Oae S (1990) Ligand coupling of 2-pyridyl sulfoxides having an sp^2 stereocenter at the α-position: a novel preparation of α-stilbazoles. Heteroat Chem 1:225–232

Westphal CH, Dipp MA, Guarente L (2007) A therapeutic role for sirtuins in diseases of aging? Trends Biochem Res 32:555–560